https://doi.org/10.5194/amt-2020-286
Preprint. Discussion started: 7 September 2020

Atmospheric Measurement Techniques Discussions

Real-world measurement and mechanical-analysis-based-verification of NO_x and CO_2 emissions from in-use heavy-duty vehicle

Hiroo Hata[1], Kazuo Kokuryo[2], Takehiko, Ogata[2], Masahiko Kugata[1], Koichi Yanai[1], Megumi Okada[1], Chikage Funakubo[1], Minoru Yamazaki[1], Junya Hoshi[1]

[1]Tokyo Metropolitan Research Institute for Environmental Protection 1-7-5, Sinsuna, Koto-ku, Tokyo 136-0075, Japan
[2]Modern Planning Inc. 5-49-10 Chuo, Nakano-ku, Tokyo 164-0011, Japan

Correspondence to: Hiroo Hata (hata-h@tokyokankyo.jp)

Abstract. A portable emission measurement system (PEMS) was used to measure the real-world driving emissions pertaining to a Japanese middle-sized heavy-duty vehicle. The testing was performed with the vehicle being driven in the metropolitan area of Tokyo in four seasons (January, June, August, and November) to analyze the seasonal dependence of NO_x and CO_2 emissions. The experimental results indicated that the amount of NO_x emissions was particularly high in the cold season, owing to the slow starting of the NO_x detoxification systems, that is, the exhaust gas recirculation and urea-selective-catalytic-reduction systems, under low ambient temperature conditions. In the real-world driving, a high acceleration pattern was observed in the low-speed region, which is not considered in the world harmonized vehicle cycle, which is the worldwide official driving mode in the chassis dynamometer experiment. Finally, the transient emission tables for NO_x and CO_2 were constructed based on the PEMS measurement results and the classical mechanic theory. The constructed tables well replicated the experimental results in all the considered conditions involving different ambient temperatures and locations. The proposed approach can be used to evaluate emission inventories in the future.

1 Introduction

The air pollution caused by long-term and short-term air pollutants is a cause of significant concern in many countries. CO_2, which is a greenhouse gas and contributes to global warming, is a critical long-term air pollutant. According to the worldwide observation data, the global temperature has increased by approximately 1 ℃ from the average temperature from 1951–1980 (National Aeronautics and Space Administration). Global warming continues to occur, with the global temperature increasing annually, and it has been reported that if strategies to eliminate greenhouse gas emission from anthropogenic sources are not adopted, the global temperature will increase by more than 2 ℃ (Saito, 2010). In addition, photochemical oxidant is a well-known short-term air pollutant generated by the photochemical reaction of NO_x and volatile organic compounds (VOCs). The concentration of photochemical oxidant in the atmosphere is a significant concern for humans, animals, and crops in many countries (O'Neill et al., 2004; Chappelka and Samuelson, 1998; Wang et al., 2017). The Japanese government has set the environmental standard for photochemical oxidant as 0.06 ppm per hour; however, the values in all the tested sites in 2017 exceeded this standard value (Ministry of the Environment, 2017). To address the problems of global warming and photochemical pollutants, it is necessary to mitigate air pollution. In this context, heavy-duty vehicles represent a major emission source of CO_2 and NO_x (Seo et al., 2016; Seo et al., 2018; Hata and Tonokura, 2019). According to statistical reports, almost 20% of the total CO_2 and NO_x emissions in Japan are produced by heavy-duty vehicles (Ministry of the Environment, 2018), and thus, it is necessary to implement laws to reduce the exhaust emissions from heavy-duty vehicles. However, prior to setting new regulatory limits for exhaust emissions, experimental testing must be performed to understand the emission trend corresponding to the target vehicles. Until recently, the vehicle exhaust emissions were experimentally examined by conducting laboratory tests using a chassis dynamometer. The advantage of such testing is the high repeatability of each test; moreover, several types of vehicles can be tested under nearly identical conditions, such as the driving mode and environmental temperature. However, in the chassis dynamometer experiment, the change in the seasonal ambient temperature and road

https://doi.org/10.5194/amt-2020-286
Preprint. Discussion started: 7 September 2020

Atmospheric Measurement Techniques Discussions

gradient are not considered. In general, the laboratory temperature is set at approximately 25 °C, and it cannot be easily changed via the normal laboratory system. It has been noted that the environmental temperature considerably influences the amount of exhaust emissions, because the catalysis converter, which purifies the emissions from the vehicles to non-toxic components, has a specific activation temperature that cannot be attained in cold seasons, thereby leading to the release of a large amount of pollutants (including NO_x) in the atmosphere (U.S. Environmental Protection Agency). Moreover, the road gradient also influences the amount of exhaust emissions because it directly affects the driving force, which is presumed to be proportional to CO_2 and other exhaust emissions. Consequently, governments and researchers worldwide are conducting real-world exhaust emission testing by using portable emission measurement systems (PEMS). Gallus et al. (2017) measured the exhaust emissions from two diesel light-duty vehicles using PEMS and analyzed the relationship between the emission trends of CO_2 and NO_x and road properties such as the road gradient and driving style. It was noted that the road gradient linearly affected the amount of CO_2 and NO_x emissions, thereby indicating the importance of obtaining measurement from the vehicles in road tests. Mendoza-Villafuerte et al. (2017) measured the emission trend from a heavy-duty vehicle by using PEMS and developed an analysis method based on the geographic information system. The results clarified the notable influence of the road boundary condition, land-use data, and speed-limit data on the amount of emissions. Moreover, several studies were conducted using PEMS to measure the basic data from both light-duty and heavy-duty vehicles (Kousoulidou et al, 2013; Kwon et al, 2017; Liu et al, 2009; Luján et al, 2018; O'Driscoll et al, 2016). Nevertheless, the conduction of road measurement experiments using PEMS is a relatively new domain, and only a few studies have been performed to assess the analytical data, for instance, in terms of the mathematical formulation of the effect of ambient temperature on the exhaust emission and application of the measurement results to evaluate the emission inventory.

To address this aspect, in this study, chassis-dynamometer-based and real-world emission measurements using PEMS were conducted for a heavy-duty Japanese vehicle. The obtained experimental results and the theory of classical mechanics were used to develop an analytical method to evaluate the amount of CO_2 and NO_x emissions from the vehicle in an arbitrary driving condition. Moreover, the difference between chassis dynamometer and PEMS results was quantified to understand the difference in the amount of real-world emissions and laboratory measurement results. It was expected that the proposed method could be used to quantify the results of real-world exhaust emission measurements, and the analyzed data could be applied to evaluate the emission inventory from the vehicles in the future.

2 Methodology

2.1 Laboratory test using chassis dynamometer

The exhaust emission from a diesel heavy-duty vehicle in the Japanese market was measured using a chassis dynamometer (Meiden Engineering Co. MEIDACS-DY6200P). The measured vehicle was equipped with a diesel particulate filter and urea selective catalytic reduction (urea-SCR) system, and it met the current Japanese regulation set in 2016. The specifications of the vehicle are listed in Table S1. The emission components including CO, CO_2, NO, NO_2, CH_4, total hydrocarbon (THC), and N_2O were measured using the vehicle's emission measurement system (HORIBA Ltd., MEXA-7400D). In particular, the amounts of CO, CO_2, CH_4, and N_2O were measured using a nondispersive infrared sensor. The NO and NO_2 amounts were measured using the chemiluminescence method, and the amount of THC was measured using a flame ionization detector (FID). The detailed composition of the THC, including the VOCs, was measured using a gas chromatograph mass spectrometer and FID (GC-MS/FID, GCMS-QP2020, Shimadzu Corp.) and liquid chromatograph mass spectrometer (LC-MS, G6120B Quadrupole LC/MS, Agilent Technologies Inc.). The details of the VOC analysis method have been provided in our previous work (Hata et al, 2019). Although the VOC analysis is beyond the scope of this study, the information may be useful for researchers who aim to examine the composition of the VOCs emitted from heavy-duty vehicles; therefore, the analyzed data are provided as supplementary data. The tested driving mode was the world harmonized vehicle cycle (WHVC) with cold- and

https://doi.org/10.5194/amt-2020-286
Preprint. Discussion started: 7 September 2020

Atmospheric Measurement Techniques Discussions

hot-starts. Laboratory tests were conducted in all the seasons; however, VOC analyses were performed in only three seasons, that is, in November 2018, June 2019, and August 2019.

2.2 Real-world measurement using PEMS

A PEMS (HORIBA Ltd., OBS-ONE) was used to perform the road emission measurement. The measured components included CO, CO_2, NO, NO_2, and THC, and the measurement techniques were the same as those in the chassis dynamometer experiment, as described in Section 2.1. The tests were conducted in four seasons to investigate the seasonal dependence of the emissions: autumn (November 19–21, 2018), winter (January 15–17, 2019), spring (June 10–14, 2019), and summer (August 26–30, 2019). All the tests were conducted two times in one day, in the morning and afternoon. The vehicle speed, ambient temperature, humidity, exhaust gas recirculation (EGR) ratio, urea-SCR temperature, and urea injection ratio were determined using the information of an on-board device (OBD) on the vehicle. The EGR ratio was measured only in the spring and summer tests. The driving route included the city and bay area of Tokyo, with the total driving distance being 28.5 km.

2.3 Experimental data processing

2.3.1 Data smoothing of vehicle speed and acceleration

The vehicle speed (km/s) was monitored in the experimental process at 10 Hz. The vehicle acceleration (km/s^2) was calculated by determining the differential of the vehicle speed. Because the dispersion of the acceleration calculated using the data of the vehicle speed obtained at 10 Hz appeared to be large, the vehicle speed data in arbitrary time, v_t, was smoothed using Equation (1).

$$v_t = \sum_{i=t-2}^{t+2} \frac{v_i}{5} \tag{1}$$

Using the smoothed vehicle speed, the acceleration in arbitrary time, at, was calculated using the central difference method, as follows:

$$a_t \equiv \frac{dv_t}{dt} \cong \frac{v_{t+1} - v_{t-1}}{2\Delta t} \tag{2}$$

where Δt is the time step of the monitoring time duration (=0.1 s).

2.3.2 Time delay treatment between observed concentration and vehicle acceleration

The exhaust emission was measured using the analyzer installed in the chassis dynamometer or PEMS, and the OBD information was collected directly from the vehicle. Owing to the different approaches employed, the measured exhaust emission and velocity (or acceleration) involved a time delay. To compensate for this delay, a statistical method was applied. As discussed in the subsequent section, the target pollutants, NO_x and CO_2, increased when the vehicle accelerated, indicating that the concentration of the pollutants and acceleration are correlated. The cross-correlation function between two parameters x and y at time τ, $C_{xy}(\tau)$ can be defined as follows:

$$C_{xy}(\tau) = \frac{R_{xy}(\tau)}{\sqrt{R_{xx}(0)R_{yy}(0)}} \tag{3}$$

where $R_{xx}(0)$ and $R_{yy}(0)$ are the autocorrelation function of x and y in the base time, respectively, and $R_{xy}(\tau)$ is the cross-correlation function at time τ. The time τ corresponding to the maximum cross-correlation function (defined in Equation (3)) was numerically determined and defined as the time delay between the emission peak and acceleration.

2.3.3 Evaluation of driving force

The vehicle driving force, F, can be defined as follows:

https://doi.org/10.5194/amt-2020-286
Preprint. Discussion started: 7 September 2020

Atmospheric Measurement Techniques Discussions

$$F = (m + \Delta m)a + \mu_r mg + mg\sin\theta + \mu_a A v^2 \quad (4)$$

here F, m, Δm, a, μ_r, g, θ, μ_a, A, and v denote the driving force (N), weight of inertia of the vehicle (kg), weight of the rotatory parts of the vehicle (kg), vehicle acceleration (m/s^2), rotation friction coefficient, gravity due to acceleration (9.8 m/s^2), slope angle, air friction coefficient, area of the front side of the vehicle (m^2), and vehicle speed (m/s), respectively. With reference to our previous work (Kugata et al., 2012), μ_r and μ_a were set as 0.0089 and 0.0027, respectively. The threshold of acceleration was defined as 0.139 m/s^2, and if the acceleration was less than this value, the acceleration was set as zero. The vehicle weight, m, including the weight of the cargo such as PEMS, batteries, and other measurement-related parts, was set as 5880 kg. The parameter Δm, pertaining to the weight of the transmission system and tires, was set as 0.10 (during acceleration) and 0.07 (in the case of constant speed), respectively. A was set as 7.5725 m^2, as reported in a tutorial of the tested vehicle. θ was extracted from the altitude information derived from the aviation laser surveying data (ALSD) (Geospatial Information Authority of Japan). In particular, the ALSD includes the altitude information in an arbitrary area in Japan with a mesh size of less than 2×2 m. The data assessment was performed by conducting the following three steps.

・Two types of ALSD are available: original and filtered data. The original data include the complete information of the ALSD, whereas the filtered data include the ALSD information with the buildings and trees filtered to ensure that the users can assess the usable land information. The filtered ALSD were selected in this study.

・The altitude data from the ALSD were sorted into 1 m grids, and the altitude of each mesh was set considering the nearest altitude in the ALSD. These altitudes were smoothed using the mean average of 5 m meshes in the vicinity.

・Using the determined altitude, the road slope was calculated by considering the tangent of 7 m meshes in the vicinity of two meshes.

3 Results and discussion

3.1 Seasonal trend of measured NO_x emissions in real-world driving

The time profile of the NO_x emissions in four seasons is shown in Figure 1. It can be noted that the NO_x emissions in real-world driving are season-dependent and inversely proportional to the ambient temperature. According to Figure 1, the time profile of the NO_x emissions can be divided into three phases: high-emission phase from the start of the driving time to 10 min (phase 1), medium- to low-emission phase in the driving time from 10 to 30 min (phase 2), and low-emission phase in the driving time after 30 min (phase 3). These three phases are related to the operation of the EGR and urea-SCR. In general, the EGR system decreases the O_2 concentration in the intake air to reduce the amount of NO_x generated inside the engine room by recirculating the exhaust gas to the intake air (Abd-Alla, 2002). The urea-SCR system reduces the NO_x concentration in the exhaust gas through the redox reaction between NO_x and NH_3, which is produced by the hydrolysis of urea (Fang and DaCosta, 2003; Hsieh and Wang, 2011; Upadhyay and Van Nieuwstadt, 2006). The operation of the EGR and urea-SCR systems is usually avoided in the initial stage of driving, because in the cold-start process, the exhaust gas temperature and catalysis surface temperature are low, likely leading to the deposition of the particulate matter in the EGR system and urea leakage from the SCR system. Moreover, the operation of the EGR is avoided in the cold-start phase to prevent the occurrence of accidental fires in the engine room and the presence of unburned fuel. Figure S1 shows the relationship between the EGR ratio (%) and engine coolant temperature of the tested vehicle. In general, the engine coolant temperature indicates the exhaust gas temperature and is usually used to control the EGR system. Figure S1 shows that the EGR begins to operate when the engine coolant temperature reaches 60 °C. The time profile of the engine coolant temperature measured in the four seasons is shown in Figure S2. The dependence of the coolant temperature on the season (or the ambient temperature) is notable. The coolant temperature increases to 60 °C more rapidly in the hotter seasons than in the colder seasons. Therefore, the EGR system starts operating earlier in hot seasons such as summer; consequently, the amount of NO_x emissions in hot seasons is lower than that

https://doi.org/10.5194/amt-2020-286
Preprint. Discussion started: 7 September 2020

Atmospheric Measurement Techniques Discussions

in the cold seasons. Figure S3 shows the relationship between the urea injection amount and SCR surface temperature. It can be noted that the urea injection started after the SCR temperature became 150 ℃. The time profile of the SCR temperature in the real-world driving in four seasons is illustrated in Figure S4. Similar to the trend of the engine coolant temperature, the SCR temperature increases to 150 ℃ more rapidly in hot seasons than in cold seasons. Therefore, the season (or ambient temperature) influences the effectiveness of the urea-SCR system, and the NO_x emissions are thus lower in hot seasons such as summer. According to Figure 1, phase 1 corresponds to the period in which both the EGR and urea-SCR systems are not operating. In phase 2, the EGR system is operating, and the NO_x emissions are thus partly purified. In phase 3, both the EGR and urea-SCR systems are operating, resulting in a high detoxification of NO_x. These three phases considerably depend on the ambient temperatures, and colder seasons, such as winter, involve a higher amount of NO_x emissions. Figure 2(a) shows the relationship between the ambient temperature and total NO_x emissions per driving distance (g/km). According to Figure 2(a), the NO_x emissions are dominant in phase 1. The magnitude of the emissions is 2 to 7 times lower in phase 2 than that in phase 1, and nearly no emissions occur in phase 3. Thus, the cold-start emission in phase 1 is a critical phase to mitigate the amount of NO_x emissions in the atmosphere.

3.2 Measured CO_2 emissions in real-world driving

Figure 2(b) shows the relationship between the ambient temperature and total CO_2 emissions per distance (g/km). The temperature dependence of the CO_2 emissions is lower than that of the NO_x emissions. In some cases, after the EGR started operating, the CO_2 emission was high; however, this phenomenon likely occurred owing to the error of the driving pattern in each real-world driving test. Moreover, although the amount of CO_2 emissions appears to vary with the phases defined in the previous section, it does not depend on the ambient temperature in each phase, thereby indicating that the EGR and urea-SCR systems do not influence the amount of CO_2 emissions. The driving speeds in phases 1 and 2 were lower than that in phase 3 because the road tended to be crowded in phases 1 and 2, leading to the high emission of CO_2 caused by frequent acceleration. Moreover, in the beginning of the cold-start process, the engine is cooled, and the combustion efficiency in this case is lower than that after the engine is warmed. Furthermore, in the cold-start process, the vehicle body is also cooled, and the friction of the rotatory parts of the vehicle is likely increased. Therefore, the difference in the CO_2 emissions in the three phases can be attributed to three cold-start features, difference of the vehicle speed in each phase, difference in the engine combustion efficiencies, and high rotation friction of the rotatory parts.

3.3 Comparison of NO_x and CO_2 emissions determined using PEMS and chassis dynamometer

Figure S5 shows the vehicle speed and acceleration distribution determined using the PEMS measurement and WHVC mode from the chassis dynamometer measurement divided into six torque ranges and three engine rotation ranges. In the low to middle engine rotation ranges with middle to high torque ranges, the PEMS results correspond to a high acceleration in the low vehicle speed field. This indicates that the real-world driving includes a sudden acceleration profile in the Japanese urban road, which is not taken into account by the WHVC approach. Moreover, the WHVC includes a high vehicle speed range, which does not appear in the PEMS results. In this study, the real-world driving emissions were measured on an ordinary road in the metropolitan area of Tokyo. The vehicle speed on this road in the urban area was limited to 60 km/h, and thus, data pertaining to the speeds of more than 60 km/h were not collected, because this study was focused on the NO_x and CO_2 emission trends in urban areas. Obtaining the measurements for the high-speed range is a task for future work.

The NO_x and CO_2 emissions per driving (g/km) in the four seasons, as obtained from the WHVC, are shown in Figure 3. It can be noted that the emissions were almost the same in the four seasons, indicating that the vehicle condition in each season was nearly identical; therefore, the PEMS test results in the four seasons could be considered to be comparable.

Although this study was focused on NO_x and CO_2 emissions, the emissions of other gaseous species including CO, THC, CH_4, and N_2O were also measured, as summarized in Table S1.

https://doi.org/10.5194/amt-2020-286
Preprint. Discussion started: 7 September 2020

Atmospheric Measurement Techniques Discussions

3.4 Physical analysis of NO_x and CO_2 emissions considering the vehicle speed and driving force

3.4.1 Force–speed–emission transient map

When evaluating the emission inventory from vehicles, it is necessary to formulate the emission factor of each pollutant, which can be used to evaluate the amount of emissions in arbitrary environmental conditions (in terms of the time, location, ambient temperature etc.). Some researchers have attempted to formulate the amount of emissions from vehicles, based on PEMS experiments (Bishop et al, 2019) and the vehicle specific power method (Koupal et al, 2005). However, in the case of heavy-duty vehicles, the detoxification system is complex, and the formulation of the pollutants' emissions involves high variability. To eliminate this variability from the estimation model, a transient emission table was constructed in this work. The formulation method was based on the assumption that the amount of emissions such as those of NO_x and CO_2 depend on the driving force and vehicle speed at any given moment. Because this dependence cannot be formulated mathematically, an emission table containing the parameters of the driving force, vehicle speed, and amount of emissions was employed. The driving force was calculated using Equation (4). The obtained transient table for the NO_x and CO_2 emission generated by the tested vehicle and measured by PEMS in the real-world driving is shown in Figures 4 and 5, respectively. As shown in Figure 4, the amount of NO_x emissions is proportional to the driving force and vehicle speed and inversely proportional to the ambient temperature, as discussed in a previous section. The amount of NO_x emissions decreases when the two NO_x detoxification systems, EGR and urea-SCR, start operating. According to Figure 5, the CO_2 emissions increase in proportion to the driving force and vehicle speed; however, the amount of emissions is not considerably influenced by the ambient temperature, because the ambient temperature mainly affects the detoxification catalysis activity. After the EGR and urea-SCR start operating, the amount of CO_2 emissions in the low-temperature condition is lower than that in high-temperature conditions. When the measurement tests were conducted in the summer season, the air conditioner was switched on, and it was considered that the temperature dependence after the two NO_x detoxification systems started operating likely results from the use of the air conditioner. The difference in the CO_2 emissions before and after the EGR and urea-SCR start operating is lower than that of the NO_x emission. In phase 1, the driving situation is similar to the cold-start, and insufficient fuel combustion occurs. However, in phase 3, the driving situation is almost similar to that of a hot-start, and the fuel combustion efficiency is maximized, resulting in lower CO_2 emissions. Using the transient tables mapped in Figures 4 and 5, the NO_x and CO_2 emissions from a test vehicle in an arbitrary driving pattern with an arbitrary temperature and road gradient can be predicted. Figure 6 shows the comparison between the NO_x and CO_2 emissions determined experimentally via PEMS measurement and the values estimated from the transient emission tables mapped in Figures 4 and 5. The transient table values agree with the experimental results, with a correlation factor of 0.9. The results shown in Figure 6 indicate that once the emission profiles of NO_x and CO_2 have been obtained using a real-world driving method with detailed road information such as the ambient temperature and road gradient, the emissions in the arbitrary conditions can be well predicted, and these estimates can be used to evaluate the emission inventory. This aspect also applies to the profiles of other pollutants such as CO and HC; however, these pollutants are not the focus of this study.

Moreover, in future work, the evaluation must be performed considering the high-speed range (more than 60 km/h) and more test vehicles. In this study, the real-world driving emission tests were conducted only in the urban area of Tokyo; however, the test must also be conducted on an express highway to determine the pollutants' emissions in the high-speed range to evaluate the complete Japanese emission inventory. Furthermore, the emissions of only one heavy-duty vehicle were measured in this work. In future testing, several other types of vehicles must be considered to obtain a statistically valid inventory.

3.4.2 Sensitivity analysis of driving force

The evaluated transient map indicated that the driving force directly influences the amount of NO_x and CO_2 emissions. According to Equation (4), the driving force includes three parameters that are related to the vehicle operation: acceleration,

https://doi.org/10.5194/amt-2020-286
Preprint. Discussion started: 7 September 2020

Atmospheric Measurement Techniques Discussions

road gradient, and vehicle speed. To evaluate the parameters that considerably influence the driving force in real-world driving, a sensitivity analysis was conducted based on the following sensitivity formulas derived using the partial differential of the three parameters:

$$\frac{\partial F}{\partial a} = m + \Delta m \quad (5)$$

$$\frac{\partial F}{\partial \theta} = mg\cos\theta \quad (6)$$

$$\frac{\partial F}{\partial v} = 2\mu_a A v \quad (7)$$

Equations (5), (6), and (7) indicate the sensitivities of the acceleration, road gradient, and vehicle speed, respectively. The definitions and values of the constant parameters related to the tested vehicle have been described in Section 2.3.3. According to Equation (5), the sensitivity of the driving force to the acceleration is constant at 6468 N/(m s^{-2}). According to Equation (6), the sensitivity of the driving force to the road gradient depends on the cosine of the road gradient. The minimum and maximum absolute values of the road gradient in the driving course considered in this work were 0 and 6.8%, respectively, corresponding to a driving force sensitivity of 57624 and 57541 N, respectively. According to Equation (7), the sensitivity of the driving force to the vehicle speed is dependent on the vehicle speed. The minimum and maximum vehicle speeds in the driving process in this work were 0 and approximately 70 km/h, corresponding to sensitivities of 0 and 0.80 N/(m s^{-1}), respectively. Based on the three sensitivity factors, the road gradient most notable influences the driving force and leads to an increase in the NO_x and CO_2 emissions, as discussed in Section 3.4.1. In the laboratory test using the chassis dynamometer, the WHVC driving mode is currently applied worldwide. Although this mode includes the parameter of the road gradient, the road gradient strongly depends on the road characteristics, and therefore, it may be difficult to replicate the exhaust emission trend in a large area when using this approach. Real-world driving emission monitoring is thus meaningful to evaluate the emissions in each specific area.

4 Conclusions

Real-world driving emission experiments for a heavy-duty vehicle in the Japanese market were conducted using PEMS, and the NO_x and CO_2 emission trends were analyzed. The experimental results indicated that the amount of NO_x emissions was higher in colder seasons owing to the effect of the two NO_x detoxification systems, EGR and urea-SCR. These systems starting operating earlier in warm seasons than in cold seasons, leading to a larger amount of emissions in colder seasons. The CO_2 emissions did not exhibit an apparent seasonal dependence; however, the amount of CO_2 emissions was relatively larger in colder season owing to the low engine combustion efficiency caused by the low ambient temperature. The speed and acceleration distributions pertaining to real-world driving tests using PEMS and WHVC driving mode from the chassis dynamometer experiments indicated that the real-world driving in the urban area of Tokyo included a high acceleration in the low speed range, which is not reflected in the WHVC driving mode. The transient emission tables for NO_x and CO_2 were constructed based on the experimental results and classical mechanic theory, which well replicated the PEMS experimental results. Consequently, these tables could be used to evaluate the NO_x and CO_2 emission inventories. The results of the sensitivity analysis for the driving force suggested that the road gradient most notably influences the amount of NO_x and CO_2 emissions, thereby demonstrating the importance of conducting real-world driving emission measurements, which take into account the road characteristics in a specific area.

Author contributions. HH, MK, MY, and JH designed the research. HH, MK, KY, MO, CF, MG, and MY performed the experiments. KK and TO analyzed the statistical data. HH, KK, and TO analyzed the experimental data. HH wrote the paper.

https://doi.org/10.5194/amt-2020-286
Preprint. Discussion started: 7 September 2020

Atmospheric Measurement Techniques Discussions

Competing interest. The authors declare no conflicts of interests.

Acknowledgements. This study was funded by the Bureau of Environment, Tokyo Metropolitan Government.

References

Abd-Alla. H. G.: Using exhaust gas recirculation in internal combustion engines: a review, Energy Convers. Manag., 43, 8, 1027-1042, https://doi.org/10.1016/S0196-8904(01)00091-7, 2002.

Bishop, J. D. K., Molden, N., Boies, A. M.: Using portable emissions measurement systems (PEMS) to derive more accurate estimates of fuel use and nitrogen oxides emissions from modern Euro 6 passenger cars under real-world driving conditions, Appl. Energy., 242, 942-973, https://doi.org/10.1016/j.apenergy.2019.03.047, 2019.

Chappelka, A. H. and Samuelson, L. J.: Ambient ozone effects on forest trees of the eastern United States: a review, New. Phytol., 139, 1, 91-108, https://doi.org/10.1046/j.1469-8137.1998.00166.x, 1998.

Fang, H. L. and DaCosta, H. F.: Urea thermolysis and NO_x reduction with and without SCR catalysts, Appl. Catal, 46, 1, 17-34, https://doi.org/10.1016/S0926-3373(03)00177-2, 2003.

Gallus, J., Kirchner, U., Vogt, R., Benter, T.: Impact of driving style and road grade on gaseous exhaust emissions of passenger vehicles measured by a Portable Emission Measurement System (PEMS), Transp. Res. D., 52, 215-226, https://doi.org/10.1016/j.trd.2017.03.011, 2017.

Geospatial Information Authority of Japan (GSI). https://www.gsi.go.jp/ENGLISH/index.html (accessed on January 17, 2020).

Hata, H., Okada, M., Funakubo, C., Hoshi, J.: Tailpipe VOC Emissions from Late Model Gasoline Passenger Vehicles in the Japanese Market, Atmosphere, 10, 10, 621, https://doi.org/10.3390/atmos10100621, 2019.

Hata, H., Tonokura, K.: Impact of next-generation vehicles on tropospheric ozone estimated by chemical transport model in the Kanto region of Japan, Sci. Rep., 9, 1, 1-8, https://doi.org/10.1038/s41598-019-40012-y, 2019.

Hsieh, M., Wang, J.: Development and experimental studies of a control-oriented SCR model for a two catalyst urea-SCR system. Control Eng. Pract., 19, 4, 409-422, https://doi.org/10.1016/j.conengprac.2011.01.004, 2011.

Kugata, M., Koyano, S., Fujita, S., Miyazawa, T., Yokota, H.: About the difference in running resistance of diesel heavy duty vehicles of actual value and calculated value of the JE05 regulation, Research report of Tokyo Metropolitan Research Institute for Environmental Protection, 63-66, https://www.tokyokankyo.jp/kankyoken_contents/cmsup/pdf/houkoku203.pdf, 2012 (in Japanese with English title).

Koupal, J., Landman, L., Nam, E., Warila, J., Scarbro, C., Glover, E., Giannelli, R.: MOVES2004 Energy and Emission Inputs (Draft Report), EPA-420-P-05-003, 2005.

Kousoulidou, M., Fontaras, G., Ntziachristos, L., Bonnel, P., Samaras, Z., Dilara, P.: Use of portable emissions measurement system (PEMS) for the development and validation of passenger car emission factors, Atmos. Environ., 64, 329-338, https://doi.org/10.1016/j.atmosenv.2012.09.062, 2013.

Kwon, S., Park, Y., Park, J., Kim, J., Choi, K., Cha, J.: Characteristics of on-road NOx emissions from Euro 6 light-duty diesel vehicles using a portable emissions measurement system, Sci. Total. Environ., 576, 15, 70-77, https://doi.org/10.1016/j.scitotenv.2016.10.101, 2017.

Liu, H., He, K., Lents, M. J., Wang, Q., Tolvett, S.: Characteristics of diesel truck emission in China based on portable emissions measurement systems, Environ. Sci. Technol, 43, 24, 9507-9511, https://doi.org/10.1021/es902044x, 2009.

Luján, M. J., Bermúdez, V., Dolz, V., Monsalve-Serrano, J.: An assessment of the real-world driving gaseous emissions from a Euro 6 light-duty diesel vehicle using a portable emissions measurement system (PEMS), Atmos. Environ., 174, 112-121, https://doi.org/10.1016/j.atmosenv.2017.11.056, 2018.

https://doi.org/10.5194/amt-2020-286
Preprint. Discussion started: 7 September 2020

Atmospheric Measurement Techniques Discussions

Mendoza-Villafuerte, P., Suarez-Bertoa, R., Giechaskiel, B., Riccobono, F., Bulgheroni, C., Astorga, C., Perujo, A.: NO_x, NH_3, N_2O and PN real driving emissions from a Euro VI heavy-duty vehicle. Impact of regulatory on-road test conditions on emissions, Sci. Total. Environ., 609, 546-555, http://dx.doi.org/10.1016/j.scitotenv.2017.07.168, 2017.

Ministry of the Environment Webpage.: https://www.env.go.jp/press/106609.html (in Japanese, accessed on January 15, 2020).

Ministry of the Environment.: Total amount of greenhouse gas emission in Japan, 2018. https://www.env.go.jp/press/112856.pdf (in Japanese, accessed on January 15, 2020).

U.S. Environmental Protection Agency.: MOVES2014: Highway Vehicle Temperature, Humidity, Air Conditioning, and Inspection and Maintenance Adjustments. https://www.google.co.jp/url?sa=t&rct=j&q=&esrc=s&source=web&cd=1&ved=2ahUKEwjZrOKxvOzoAhWB3mEKHSJWCF0QFjAAegQIARAB&url=https%3A%2F%2Fcfpub.epa.gov%2Fsi%2Fsi_public_file_download.cfm%3Fp_download_id%3D504585%26Lab%3DOTAQ&usg=AOvVaw1oHKO1-hMuLXe2RqyY5868 (accessed on January 16, 2020).

National Aeronautics and Space Administration Webpage.: https://climate.nasa.gov/vital-signs/global-temperature/ (in Japanese, accessed on January 15, 2020).

O'Driscoll, R., ApSimon, M. H., Oxley, T., Molden, N., Stettler, E. J. M., Thiyagarajah, A.: A Portable Emissions Measurement System (PEMS) study of NO_x and primary NO_2 emissions from Euro 6 diesel passenger cars and comparison with COPERT emission factors. Atmos. Environ., 145, 81-91, https://doi.org/10.1016/j.atmosenv.2016.09.021, 2016.

O'Neill, M. S., Loomis, Dana., Borja-Aburto, V. H.: Ozone, area social conditions, and mortality in Mexico City, Environ. Res., 94, 3, 234-242, https://doi.org/10.1016/j.envres.2003.07.002, 2004.

Saito, S.: Role of nuclear energy to a future society of shortage of energy resources and global warming, J. Nucl. Mater., 398, 1-9, https://doi.org/10.1016/j.jnucmat.2009.10.002, 2010.

Seo, J., Park, J., Oh, Y., Park, S.: Estimation of total transport CO_2 emissions generated by medium-and heavy-duty vehicles (MHDVs) in a sector of Korea, Energies., 9, 8, 638, https://doi.org/10.3390/en9080638, 2016.

Seo, J., Kim, H., Park, S.: Estimation of CO_2 emissions from heavy-duty vehicles in Korea and potential for reduction based on scenario analysis, Sci. Total. Environ., 636, 1192-1201, https://doi.org/10.1016/j.scitotenv.2018.04.269, 2018.

Upadhyay, D., Van Nieuwstadt, M.: Model based analysis and control design of a urea-SCR deNOx aftertreatment system, J. Dyn. Sys., Meos., 128, 3, 737-741, https://doi.org/10.1115/1.2234494, 2006.

Wang, T., Xue, L., Brimblecombe, P., Lam, Y. F., Li, L., Zhang, L.: Ozone pollution in China: A review of concentrations, meteorological influences, chemical precursors, and effects, Sci. Total. Environ., 575, 1, 1582-1596, https://doi.org/10.1016/j.scitotenv.2016.10.081, 2017.

https://doi.org/10.5194/amt-2020-286
Preprint. Discussion started: 7 September 2020

Atmospheric Measurement Techniques Discussions

Table 1: Specifications of the vehicle tested in this study.

Manufacturer	Isuzu
Category	Heavy-duty
Fuel	Diesel
Displacement (L)	5,193
Vehicle weight (kg)	4,920
Detoxification tool	EGR, DPF, urea-SCR
Official fuel consumption (L/km)	0.128
Total driving distance (km)	27,241

https://doi.org/10.5194/amt-2020-286
Preprint. Discussion started: 7 September 2020

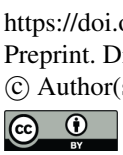

Atmospheric Measurement Techniques Discussions

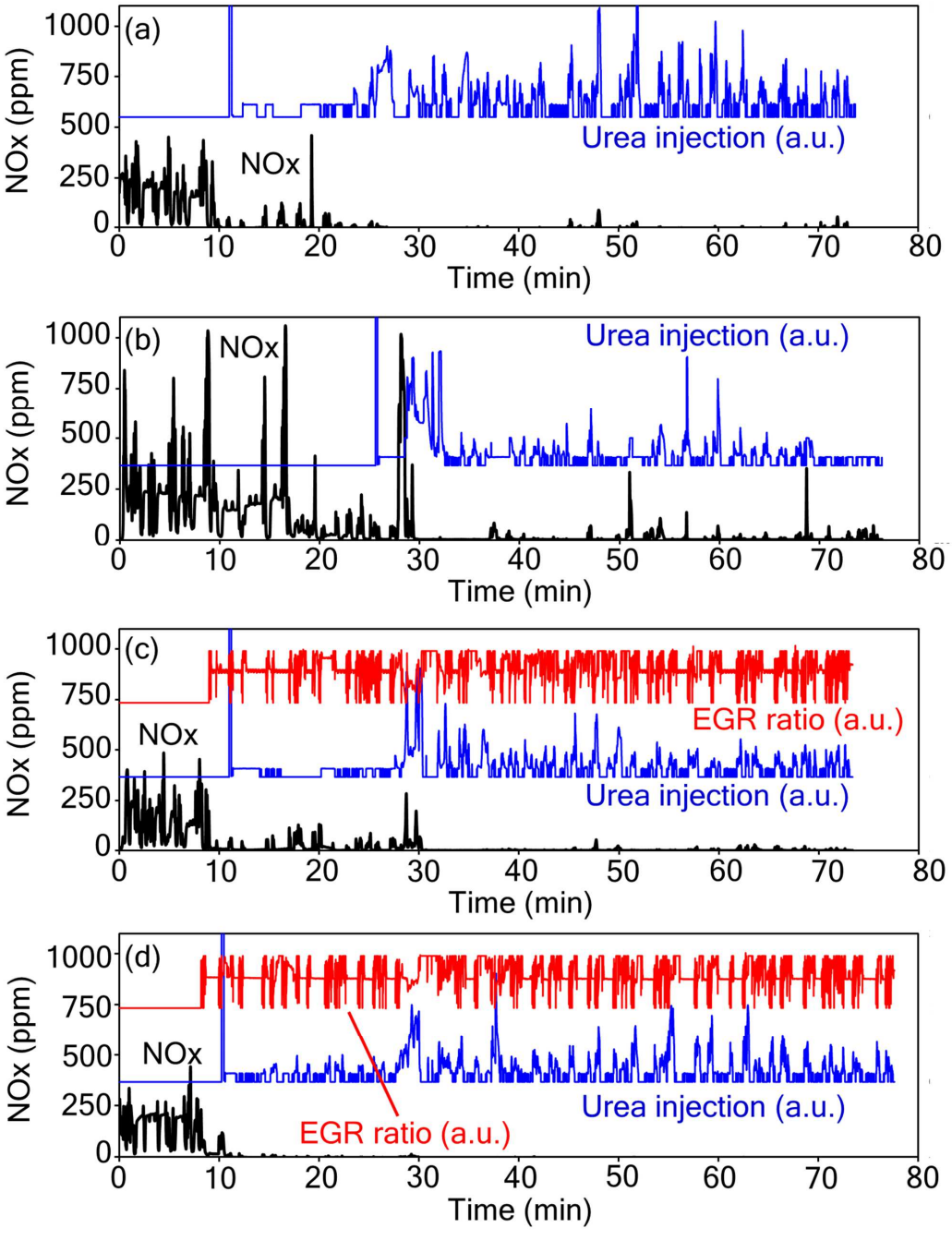

350

Figure 1: Time profiles of measured NO_x emission and driving distance in four seasons (a) autumn (November 19, 2018), (b) winter (January 15, 2019), (c) spring (June 12, 2019), and (d) summer (August 28, 2019).

https://doi.org/10.5194/amt-2020-286
Preprint. Discussion started: 7 September 2020

Atmospheric Measurement Techniques Discussions

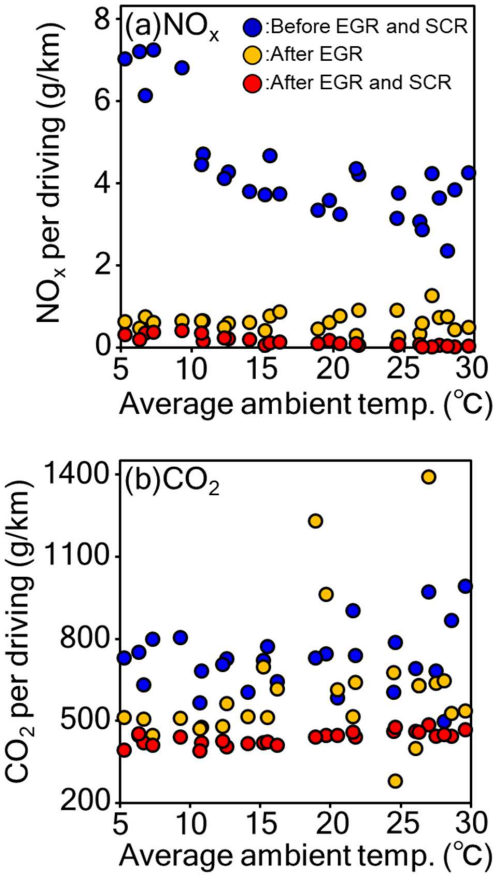

355 **Figure 2: Relationships between ambient temperature and total amount of (a) NO_x, and (b) CO_2 emissions per driving distance (g/km).**

https://doi.org/10.5194/amt-2020-286
Preprint. Discussion started: 7 September 2020

Atmospheric Measurement Techniques Discussions

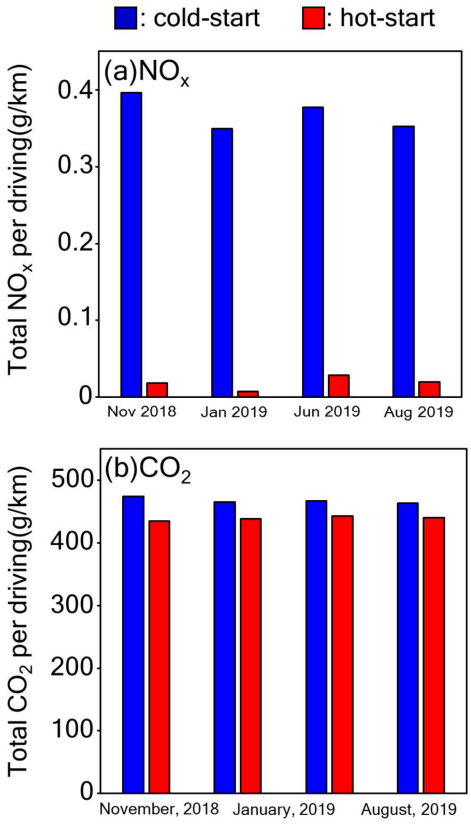

Figure 3: Experimental results of chassis dynamometer tests for world harmonized vehicle cycle cold- and hot-starts for (a) NO_x, and (b) CO_2 emissions.

https://doi.org/10.5194/amt-2020-286
Preprint. Discussion started: 7 September 2020

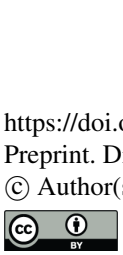

Atmospheric Measurement Techniques Discussions

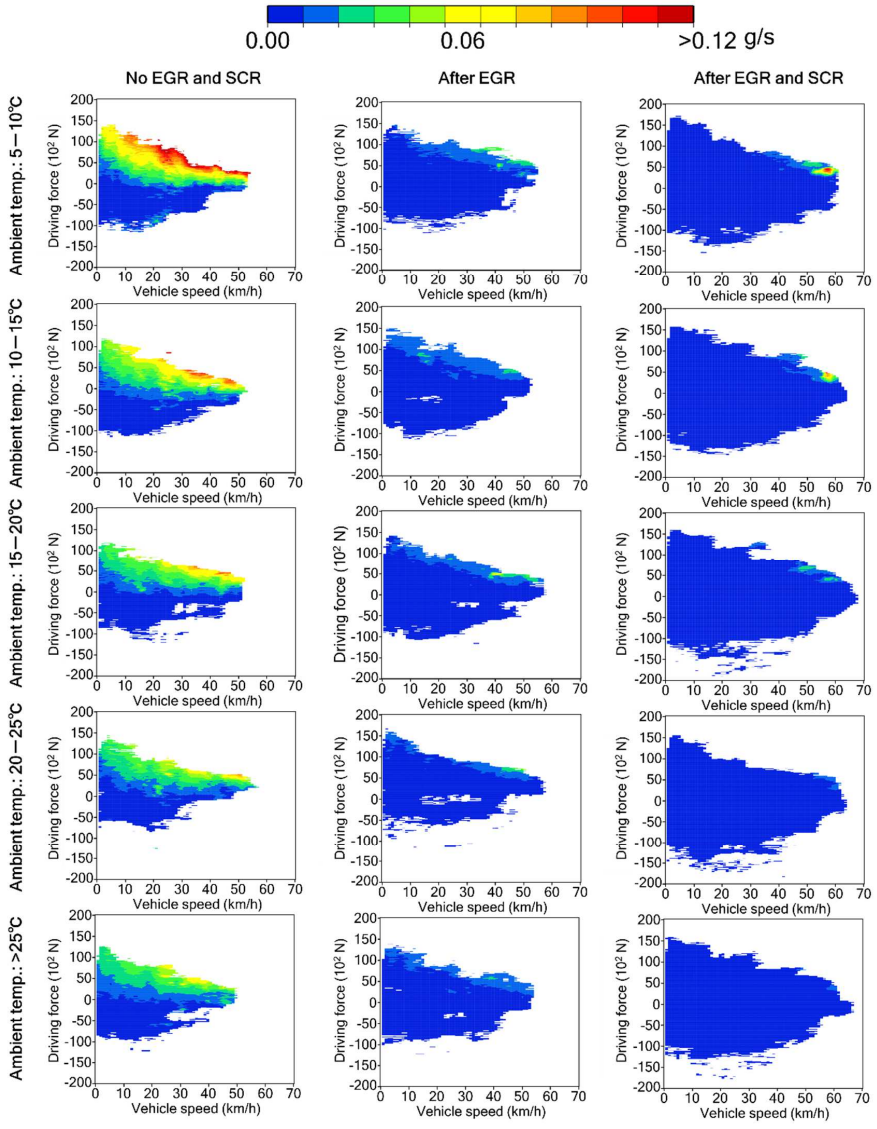

Figure 4: Transient emission map for NO_x emissions evaluated using real-world driving emission test conducted using PEMS, as well as the vehicle driving force and speed data.

365

https://doi.org/10.5194/amt-2020-286
Preprint. Discussion started: 7 September 2020

Atmospheric Measurement Techniques Discussions

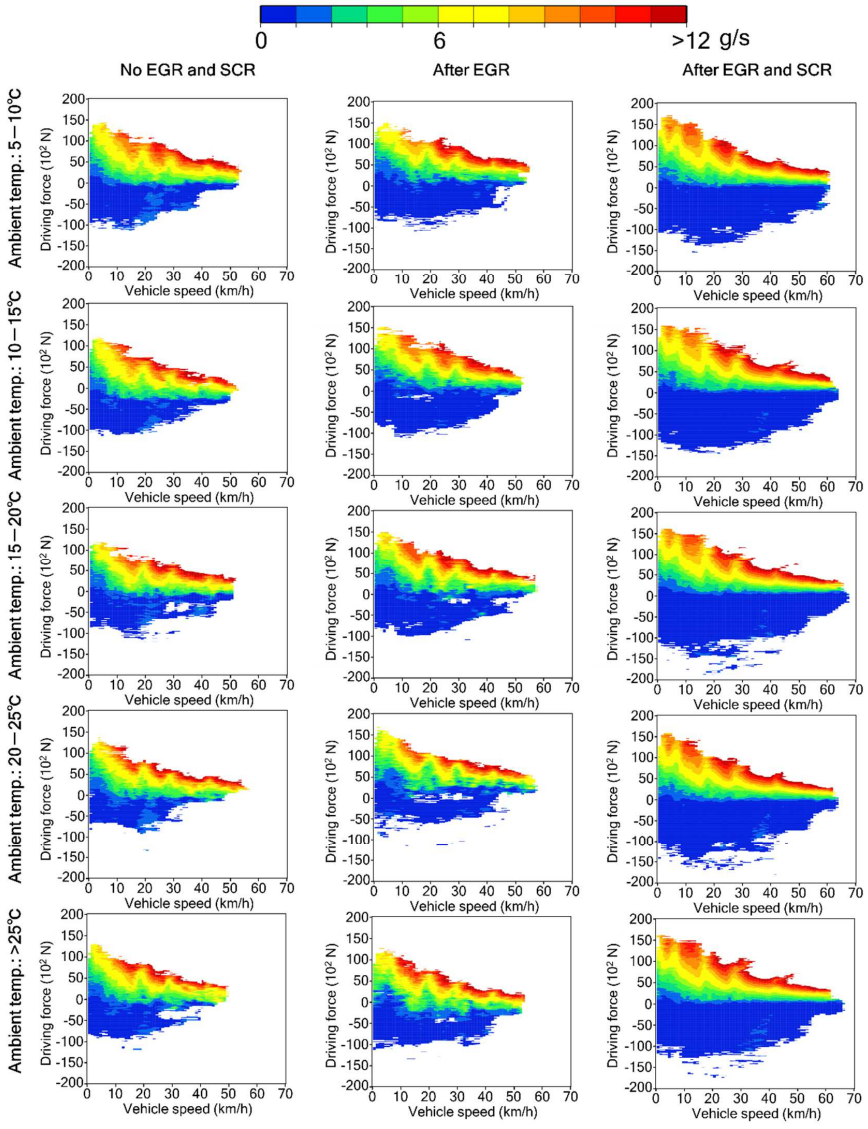

Figure 5: Transient emission map for CO_2 emissions evaluated using real-world driving emission test conducted using PEMS, as well as the vehicle driving force and speed data.

https://doi.org/10.5194/amt-2020-286
Preprint. Discussion started: 7 September 2020

Atmospheric Measurement Techniques Discussions

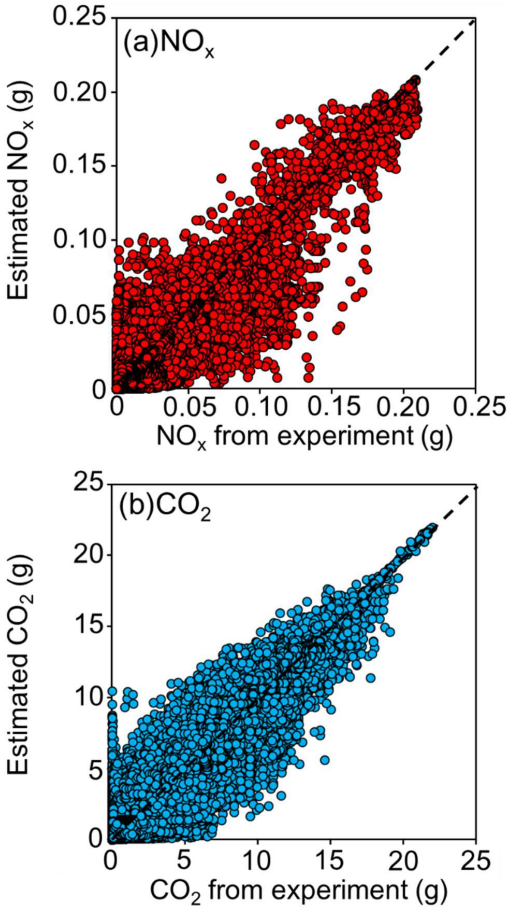

370

Figure 6: Correlation analysis of amount of (a) NO_x and (b) CO_2 emissions measured and estimated using transient tables.